Autonomic dysfunction and vasoregulation in Long COVID-19 are linked to anti-GPCR autoantibodies Parino Jan Managarian Sanda Imm

Boris Schmitz, PhD, René Garbsch, PhD, Hendrik Schäfer, MSc, Christian Bär, PhD, Shambhabi Chatterjee, PhD, Gabriela Riemekasten, MD, Kai Schulze-Forster, PhD, Harald Heidecke, PhD, Christoph Schultheiß, PhD, Mascha Binder, MD, Frank C. Mooren, MD

PII: S0091-6749(25)01128-5

DOI: https://doi.org/10.1016/j.jaci.2025.10.034

Reference: YMAI 17005

To appear in: The Journal of Allergy and Clinical Immunology

Received Date: 3 June 2025

Revised Date: 5 October 2025
Accepted Date: 15 October 2025

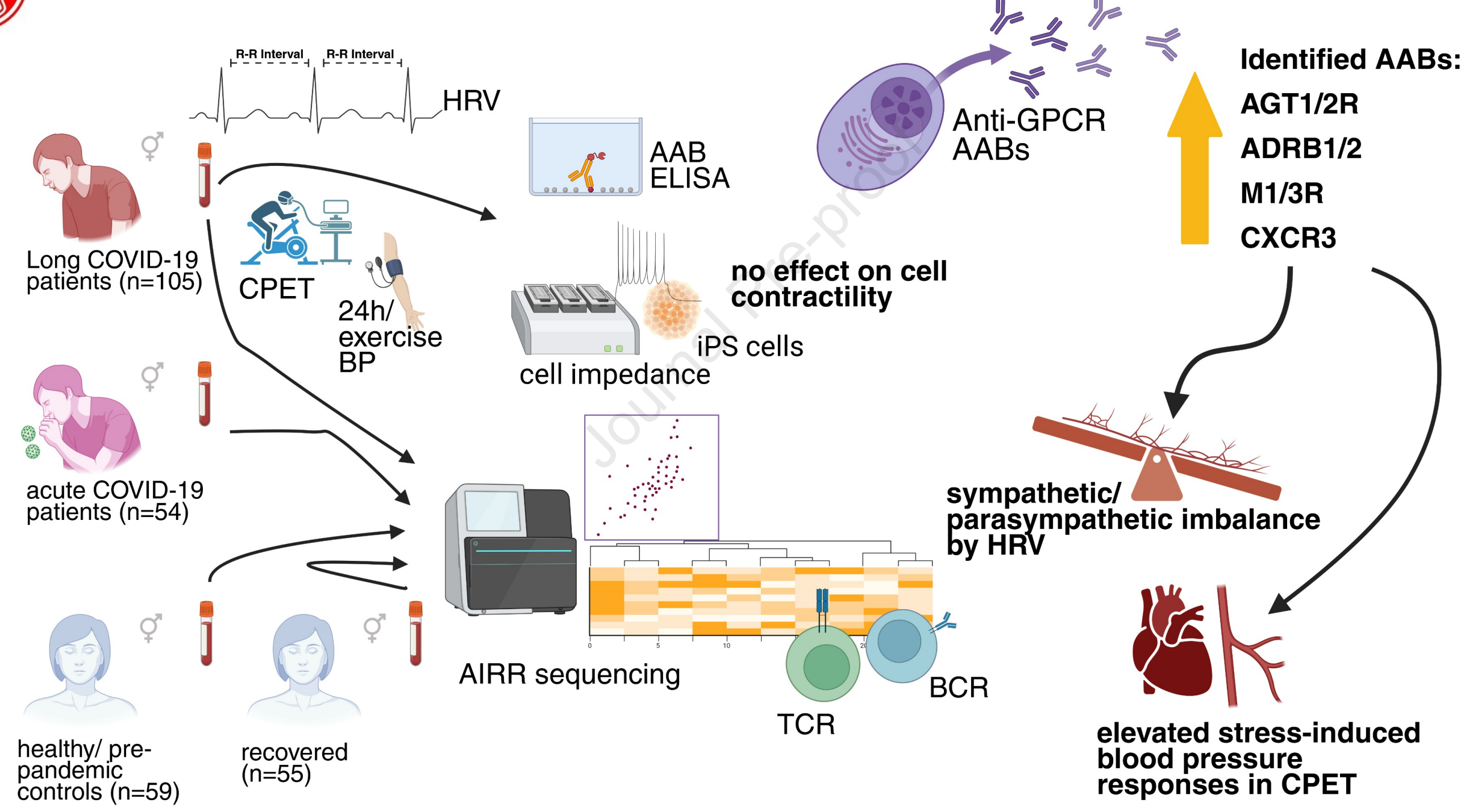
Please cite this article as: Schmitz B, Garbsch R, Schäfer H, Bär C, Chatterjee S, Riemekasten G, Schulze-Forster K, Heidecke H, Schultheiß C, Binder M, Mooren FC, Autonomic dysfunction and vasoregulation in Long COVID-19 are linked to anti-GPCR autoantibodies *The Journal of Allergy and Clinical Immunology* (2025), doi: https://doi.org/10.1016/j.jaci.2025.10.034.

This is a PDF of an article that has undergone enhancements after acceptance, such as the addition of a cover page and metadata, and formatting for readability. This version will undergo additional copyediting, typesetting and review before it is published in its final form. As such, this version is no longer the Accepted Manuscript, but it is not yet the definitive Version of Record; we are providing this early version to give early visibility of the article. Please note that Elsevier's sharing policy for the Published Journal Article applies to this version, see: https://www.elsevier.com/about/policies-and-standards/sharing#4-published-journal-article. Please also note that, during the production process, errors may be discovered which could affect the content, and all legal disclaimers that apply to the journal pertain.

© 2025 Published by Elsevier Inc. on behalf of the American Academy of Allergy, Asthma & Immunology.



Autonomic dysfunction of the Covered Vecasia Sulation in Long COVID-19 are linked to anti-GPCR autoantibodies Schmitz et al, J Allergy Clin Immunol (2025)





Abbreviations: AAB, Autoantibody; ADRB1/2, Adrenoceptor beta 1/2; AGT1/2R, Angiotensin II receptor type 1/2; AIRR, Adaptive Immune Receptor Repertoire; B/TCR – B/T-cell receptor; CPET, Cardiopulmonary exercise testing; CXCR3, C-X-C motif chemokine receptor 3; GPCR, G protein-coupled receptor; HRV, Heart rate variability; M1/3R, Muscarinic acetylcholine receptor M1/3; iPS cell, induced pluripotent stem cell.

Autonomic dysfunction and vasoregulation in

Long COVID-19 are linked to anti-GPCR autoantibodies

- Boris Schmitz, PhD^{1,2}, René Garbsch, PhD^{1,2}, Hendrik Schäfer, MSc^{1,2}, Christian Bär, PhD^{3,4,5}, Shambhabi Chatterjee, PhD^{3,4,5}, Gabriela Riemekasten, MD⁶, Kai Schulze-Forster,
- 5 PhD⁷, Harald Heidecke, PhD⁷, Christoph Schultheiß, PhD^{8,9}, Mascha Binder, MD^{8,9}, Frank C.
- 6 Mooren. MD^{1,2}

7

1

2

- ¹Department of Rehabilitation Sciences, Faculty of Health, University of Witten/Herdecke,
- 9 Witten, Germany.
- ²DRV Clinic Königsfeld, Center for Medical Rehabilitation, Ennepetal, Germany.
- ³Institute of Molecular and Translational Therapeutic Strategies (IMTTS), Hannover Medical
- 12 School, Hannover, Germany.
- ⁴Fraunhofer Institute for Toxicology and Experimental Medicine ITEM, Hannover, Germany.
- ⁵Fraunhofer Cluster of Excellence Immune-Mediated Diseases (CIMD), Hannover, Germany.
- ⁶Klinik Für Rheumatologie Und Klinische Immunologie, Universitätsklinikum Schleswig-
- 16 Holstein, Lübeck, Germany.
- ⁷CellTrend GmbH, Luckenwalde, Germany.
- ⁸Division of Medical Oncology, University Hospital Basel, Basel, Switzerland.
- ⁹Laboratory of Translational Immuno-Oncology, Department of Biomedicine, University and
- 20 University Hospital Basel, Basel, Switzerland.

21 22

23

Corresponding author:

- 24 Prof. Dr. Frank C. Mooren
- 25 Klinik Königsfeld
- 26 Holthauser Talstraße 2
- 58256 Ennepetal
- 28 Germany
- 29 Phone: +49 02333 9888 100
- 30 Email: Frank.Mooren@uni-wh.de
- 31 ORCID: 0000-0002-0258-2732

32

33

34

Competing interests

- 35 BS has received speaker honoraria from Biotronik unrelated to this work. KSF and HH are co-
- 36 founders of CellTrend GmbH. All other authors declare no competing interests.

38	ABSTR	ACT

39

40 Background

- 41 SARS-CoV-2-triggered autoantibodies (AAB) targeting G protein-coupled receptors (GPCRs)
- have been suggested to contribute to the post-acute sequelae of COVID-19 (Post-COVID-19
- 43 Syndrome, PCS).
- 44 Objective
- 45 To characterize AABs involved in autonomic dysfunction such as rhythm control and
- vasoregulation in patients with post-acute sequelae of COVID-19 and profile the peripheral B-
- and T-cell receptor (B/TCR) architecture to identify immunogenetic imprints of autoimmunity.
- 48 Methods
- 49 Anti-GPCR AABs were characterized in patients with post-acute sequelae of COVID-19 with
- 50 known alteration in autonomic nervous system functions assessed by heart rate variability
- 51 (HRV). Adaptive immune receptor repertoire sequencing (AIRR-seq) was used to profile
- 52 peripheral BCR and TCR architecture. COVID-19 patients with severe or moderate acute
- disease, after recovery, and pre-pandemic healthy individuals served as controls. Cardio- and
- vasoactive effects of AABs were analyzed using 24h and exercise test blood pressure
- 55 measurements. The direct effect of AABs on electromechanical coupling was tested in human
- 56 induced pluripotent stem cell cardiomyocytes.
- 57 **Results**
- 58 AABs including AGT1/2Rab, ADRB1/2ab, M1/3Rab, and CXCR3ab were associated with
- 59 HRV alterations. Analysis of the broad BCR repertoire metrics revealed high similarity between
- 60 PCS patients and healthy controls for clonality and diversity measures. The level of somatic
- 61 hypermutation as proxy for antigen-experience was equal to healthy controls. Elevated
- 62 CXCR3ab levels were linked to higher 24h mean arterial pressure, while patients with elevated
- 63 M1Rab and CXCR3ab levels showed higher blood pressure during stress tests. AABs had no
- effect on beat frequence and amplitude of cardiomyocyte contraction *in vitro*.
- 65 Conclusions
- 66 These findings suggest that AABs play a modulatory role in sympathetic nervous system-
- 67 mediated regulation of cardiac rhythm and vascular function in PCS. AAB levels did not
- 68 correlate with B- and T-cell receptor repertoire metrics or TRBV gene usage.

69

- 70 **KEYWORDS:** Post-acute sequelae of COVID-19; dysautonomia; autoimmunity; heart rate
- variability; G protein-coupled receptors

72	Key Messages
73	
74 75	 Anti-GPCR autoantibodies in PCS patients affect the autonomic nervous system as indicated by altered rhythm control and vasoregulation
76 77	 Autoantibodies against the CXCR3 receptor may prevent parasympathetic activation in PCS patients mainly at night
78 79	 PCS patients with higher autoantibody levels against AGTR1, M1 and CXCR3 showed elevated stress-induced blood pressure responses
80	
81	

82 Capsule Summary

- 83 In patients with Post-COVID-19 Syndrome (PCS), GPCR autoantibodies associate with
- parasympathetic tone, sympathetic predominance, and stress-induced blood pressure response,
- suggesting a modulatory role in cardiac rhythm and vascular regulation.

86 Abbreviations used

87	AAB - Autoantibody
88	ACE - Angiotensin-converting enzyme
89	ADRA1ab - Autoantibody against adrenoceptor alpha 1
90	ADRA2ab - Autoantibody against adrenoceptor alpha 2
91	ADRB1ab - Autoantibody against adrenoceptor beta 1
92	ADRB2ab - Autoantibody against adrenoceptor beta 2
93	AGT1Rab - Autoantibody against angiotensin II receptor type 1
94	AGT2Rab - Autoantibody against angiotensin II receptor type 2
95	AIRR-seq - Adaptive Immune Receptor Repertoire sequencing
96	AUC - Area under the ROC curve
97	BCR – B-cell receptor
98	BP - Blood pressure
99	CDR3 - Complementarity-determining region 3
100	CPET - Cardiopulmonary exercise testing
101	CXCR3 - C-X-C motif chemokine receptor 3
102	CXCR3ab - Autoantibody against C-X-C motif chemokine receptor 3
103	DBP - Diastolic blood pressure
104	ECG - Electrocardiogram
105	ELISA - Enzyme-linked immunosorbent assay
106	ETARab - Autoantibody against endothelin receptor A
107	GPCR - G protein-coupled receptor
108	GSK3β - Glycogen synthase kinase 3 beta
109	Gαi - Gi alpha G-protein subunit
110	HF - High-frequency band power

111	HFnu - Normalized high-frequency power
112	hiPSC - Human induced pluripotent stem cell
113	HRV - Heart rate variability
114	IGH - Immunoglobulin heavy chain
115	IGHV - Immunoglobulin heavy variable
116	IGHVJ - Immunoglobulin heavy variable/joining gene usage
117	IFNAR - Interferon- α/β receptor
118	IP-10 - Interferon-inducible protein of 10
119	IWP2 - Wnt signaling inhibitor
120	LDL - Low-density lipoprotein
121	LF - Low-frequency band power
122	LF/HF - Low-to-high frequency power ratio
123	LFnu - Normalized low-frequency power
124	MAP - Mean arterial pressure
125	ME/CFS - Myalgic encephalomyelitis / chronic fatigue syndrome
126	MFI - Multidimensional Fatigue Inventory
127	M1Rab - Autoantibody against muscarinic acetylcholine receptor M1
128	M2Rab - Autoantibody against muscarinic acetylcholine receptor M2
129	M3Rab - Autoantibody against muscarinic acetylcholine receptor M3
130	M4Rab - Autoantibody against muscarinic acetylcholine receptor M4
131	M5Rab - Autoantibody against muscarinic acetylcholine receptor M5
132	NN - Normal-to-normal (inter-beat) intervals
133	NN50 - Count of NN interval differences > 50 ms
134	PAR1ab - Autoantibody against proteinase-activated receptor 1
135	PCS – Post-COVID-19 Syndrome
136	RMSSD - Root mean square of successive differences

137	ROC - Receiver operating characteristic
138	SARS-CoV-2 - Severe Acute Respiratory Syndrome Coronavirus 2
139	SBP - Systolic blood pressure
140	SD1 - Poincaré plot short-axis dispersion
141	SD2 - Poincaré plot long-axis dispersion
142	SDANN - Standard deviation of the averages of NN intervals
143	SDNN - Standard deviation of all NN intervals
144	SDNN-Index - Mean of 5-min segment SDs of NN intervals
145	SPO2 - Peripheral oxygen saturation
146	TCR – T-cell receptor
147	TRBV – T-cell receptor beta variable
148	VAI - Angular dispersion index (Poincaré)
149	VCO2 - Carbon dioxide production
150	VDJ - Variable–Diversity–Joining
151	VE - Minute ventilation
152	VLF - Very-low-frequency band
153	VLI - Vector length index
154	VO2 - Oxygen consumption
155	W - Workload (watts)
156	

INTRODUCTION

157

158

159

160

161

162

163

164

165

166

167

168

169

170

171

172

173

174

175

176

177

178

179

180

181

182

183

184

185

186

187

188

189

Post-acute sequelae of COVID-19, also known as Post-COVID-19 Syndrome (PCS), manifests after an acute infection with the SARS-CoV-2 virus (COVID-19 infection). By definition, Long-COVID is an umbrella term for symptoms that persist ≥4 weeks after the start of acute COVID-19, while PCS refers to symptoms that continue ≥12 weeks. (1,2). Although recent guidelines propose diagnostic criteria for PCS (1,2), ambiguity persists due to the complex symptomatology and the lack of definitive diagnostic tools (3). PCS is a multisystemic disorder characterized by symptoms including but not limited to (chronic) fatigue, diminished physical performance, muscle weakness and pain, dyspnea, cognitive impairment and alterations of the autonomous nervous system, as well as psychological distress (2–5). The severity of symptoms varies widely, from mild impairment to significant restrictions in daily activities, potentially leading to partial or complete work incapacity (6). Despite ongoing investigations, the mechanisms contributing to the onset and severity of PCS remain largely unknown. Factors may include endothelial dysfunction and detrimental effects on the microvasculature, as well as a "cytokine storm" during the acute course of the infection associated with excessive oxidative stress, neutrophils programmed cell death (NETosis) and subsequent mitochondrial dysfunction (7-10). It has been suggested that PCS signs and symptoms are linked to a disruption of the autonomic nervous system associated with increased sympathetic activity (5). While the main mechanisms leading to these observations are still a matter of ongoing research, it has been reported that SARS-CoV-2 shares features of known neurotropic viruses which cause dysautonomia through dysregulation of central and peripheral autonomic circuits via direct or indirect routes including retrograde axonal transport via the olfactory nerve or the enteric nervous system (11-13). In addition to neurohormonal (over)stimulation, dysregulation of the angiotensin-converting enzyme (ACE) axis has been reported (14). As a result, sustained blood pressure deteriorations (15) and persistent or secondary autonomic dysfunction may occur, which have been suggested to add to PCS-specific symptoms including fatigue (5). We recently reported that heart rate variability (HRV) as a marker of autonomic nervous dysfunction is altered in long-term PCS patients compared with healthy controls, indicated primarily by frequency-related and nonlinear HRV variables (5). Of note, HRV alterations were more pronounced in patients with greater acute COVID-19 infection severity as well as those patients with stronger impairment of physical exercise capacity. HRV analysis showed a disturbance of day-night autonomic activity possibly indicating an impaired recovery during sleep (5). Together, these findings suggested that sympathovagal imbalance is still present in

long-term PCS patients. To what extent autonomic dysfunction in PCS can be linked to 190 autoimmune reactions triggered during the acute infection is currently largely unknown. 191 However, there is evidence that elevated autoantibody (AAB) levels against central components 192 in different regulatory systems caused by an acute COVID-19 infection may persist in PCS 193 patients (16-18). This includes prothrombotic AABs against anti-phospholipid and anti-type I 194 interferon (19,20) as well as vaso- and immunomodulatory proteins (18,21,22). Additionally, 195 AABs against vasoregulatory ACE2 and angiotensin type-1 receptor (AGTR1) have been 196 correlated with disease severity in acute COVID-19 patients (21). Of note, AABs targeting G 197 protein-coupled receptors (anti-GPCR AABs) detected in PCS patients have been proven to 198 have functional capacity, underlining their role in PCS pathology (18). Finally, the role of anti-199 200 GPCR AABs has been observed in various autoimmune and non-autoimmune diseases (23) and they have been associated with key symptoms of fatigue and muscle pain in ME/CFS patients 201 202 (24).Thus, this study aimed to identify AABs targeting GPCRs involved in autonomic regulation 203 204 such as rhythm control and vasoregulation in patients with PCS. Adaptive immune receptor repertoire sequencing was used to profile the peripheral B- and T-cell receptor architecture and 205 identify potential immunogenetic imprints of autoimmunity. The direct effect of anti-GPCR 206 AABs on electromechanical coupling was analyzed in vitro using induced pluripotent stem cell-207 derived cardiomyocytes. 208

MATERIALS AND METHODS

Study design

209

210

211

212

213

214

215

216

217

218

219

220

221

222

223

224

225

226

227

228

229

230

231

232

233

234

235

236

237

To identify anti-GPCR AABs contributing to autonomic dysfunction in PCS, AAB levels of PCS patients who had been screened using Holter ECG systems to assess HRV over at least 24h were analyzed. Included patients (n=105) were participants of a prospective cohort study, referred to Clinic Königsfeld, center for medical rehabilitation between May 2021 and April 2022 (5). Compared to healthy controls, these patients showed signs of sympathovagal imbalance. Inclusion criteria were a history of (at least one) COVID-19 infection (positive PCR test at the time of infection), and ongoing or newly expressed performance deficits lasting for at least 3 months prior to recruitment as described in detail elsewhere (5). The current study was conducted in two phases, an initial discovery phase and a second in-depths analysis phase, to reduce the number of anti-GPCR AABs analysed in the entire cohort. During the discovery phase, 14 AABs previously described in PCS or elevated in acute COVID-19 patients were selected based on respective targets involved in the regulation of parasympathetic, adrenergic, vasoactive, thrombotic and inflammatory pathways (18, 22, 25). Levels were initially compared between patients with highest (top 20%, n=22) and lowest (lowest 20%, n=22) sympathicus activation determined based on normalized HF (HFnu) over 24h. This was done based on the key finding that the frequency-related variable HFnu differed significantly in PCS patients compared to controls (5). Suggestive AABs were then tested in the entire cohort (n=105) for association with individual HRV parameters. A study flow chart is provided in Supplemental Table 1 of the Online Repository.

Patients

Patients with full clinical assessment and performance deficits documented according to the recent consensus statement, with the cluster of lead symptoms including fatigue/exercise intolerance, shortness of breath, and cognitive dysfunction (5) were included. History of comorbidities and current medication were documented and blood samples for genomic DNA sequencing and AAB analysis were drawn on the day of admission. Patients provided the respective clinical data after discharge for scientific use.

Ethical approval

- The study was approved by the local ethical review committee (Ethik-Kommission Universität
- Witten/Herdecke; reference number 159/2021) and conformed to the Declaration of Helsinki.
- 240 Written informed consent was obtained from all participants.

Determination of autoantibodies (AAB)

241

257

258

259

260

261

262

263

264

265

266

267

268

269

270

271

272

273

Whole blood samples were allowed to clot at room temperature and then centrifuged at 2000 x 242 g for 15 min in a serum gel monovette. The serum was aliquoted and, together with the 243 remaining cellular fraction, stored at -80°C. IgG AAB against Angiotensin II receptor 1 and 2 244 245 (AGT1Rab, AGT2Rab), Adrenoceptor Alpha 1 and 2 (ADRA1ab, ADRA2ab), Adrenoceptor Beta 1 and 2 (ADRB1ab, ADRB2ab), Muscarinic Acetylcholine receptor M1-5 (M1Rab, 246 M2Rab, M3Rab, M4Rab, M5Rab), Endothelin Receptor A (ETARab), Proteinase-activated 247 receptor 1 (PAR1ab), and CXC Motif Chemokine receptor 3 (CXCR3ab) were measured using 248 respective sandwich ELISA kits by CellTrend GmbH (Luckenwalde, Germany) in an EN ISO-249 certified laboratory (CellTrend) as described (18, 22). In brief, serum samples were diluted at a 250 1:100 ratio and AAB levels were calculated as arbitrary units (U) by extrapolating from the 251 standard curve. The ELISA kits were validated in accordance with the Food and Drug 252 Administration's Guidance for Industry: Bioanalytical Method Validation and intraassay 253 coefficient of variation ranged from 3.9% to 15.2% depending on the respective assay. PCS 254 patients' AAB levels were compared to internal reference based on normal values of healthy 255 individuals. 256

Assessment of Heart Rate Variability (HRV) and long-term blood pressure

HRV was assessed using 24h Holter ECG (DMS300-4L, DM systems, Beijing, China) and the following variables were extracted for analyses as described (26). Frequency domain variables (HF, average energy density in the high-frequency band [i.e., between 0.15 and 0.4 Hz of all 5min-calculation windows]; LF, average energy density in the LF low-frequency band [i.e., between 0.04 and 0.15 Hz of all 5-min-calculation windows]; HFnu, normalized HF [HF/(total power-VLF)*100]; LFnu, normalized LF [LF/(total power-VLF)*100]; HF power [absolute power of the HF band]; LF power [absolute power of the LF band]), time domain variables (NN intervals, SDNN, standard deviation of all NN intervals; SDNN-Index, mean value of the standard deviations of the average NN intervals of all 5-min segments of a measurement; SDANN, standard deviation of the average NN intervals of all 5-min segments of a measurement; RMSSD, square root of the mean of the sum of the squares of differences between adjacent NN intervals; pNN50, NN50 divided by the total number of NN intervals; triangular-Index, integral of the NN interval histogram divided by the height of the histogram), nonlinear variables as defined by the analysis of Poincaré maps, a scatter plot of inter-beat intervals as a function of previous inter-beat intervals (SD1, the standard deviation of Poincaré plot perpendicular to the line-of-identity; SD2, the standard deviation of the Poincaré plot along

- 274 the line-of-identity; VAI, the angular dispersion of scatter points; VLI, the vector length index).
- 275 Long-term (24h) blood pressure measurements were performed as part of the clinical routine
- using Physio-Port (PAR Medizintechnik, Berlin, Germany) and PhysioQuantWin 7.0 (EnviteC-
- 277 Wismar, Germany). Mean arterial pressure (MAP) was approximated using the formula MAP=
- 278 (2*DBP+SBP)/3.

279

Cardiopulmonary exercise testing (CPET)

- 280 Symptom-limited ergometer testing with continuous breath-by-breath respiratory gas exchange
- analysis was conducted following manufacturer's guidelines (Ergostic, Amedtec, Aue,
- Germany) as part of the standard clinical diagnostic procedure upon admission and within three
- 283 days prior to discharge as described in detail elsewhere (27). Expiratory flow measurements
- were performed using a mass flow sensor, calibrated with a known concentration gas mixture
- prior to each assessment. Continuously recorded variables included workload (W), heart rate
- 286 (HR), blood oxygen saturation (SPO₂), blood pressure (BP), oxygen consumption (VO₂),
- 287 carbon dioxide production (VCO₂), and minute ventilation (VE). For comparability of BP and
- SPO₂, data were normalized to the maximal load, with the individual maximum power set to
- 289 100% with BP and SPO₂ assigned to the corresponding percentage of the load.

290 Adaptive immune receptor repertoire sequencing (AIRR-seq)

- 291 Genomic DNA was isolated from fresh-frozen peripheral blood using the GenElute mammalian
- 292 genomic DNA miniprep kit (Sigma-Aldrich, Taufkirchen, Germany) from PCS patients (n=34)
- 293 stratified by overall AAB levels and HFnu values (28). Immunogenic control data from
- 294 COVID-19 patients with severe (n=26) or moderate (n=28) acute disease and after recovery
- 295 (n=55) as well as pre-pandemic healthy individuals (n=59) was used. Patients and healthy
- 296 control characteristics are given in Supplemental Table 1 of the Online Repository including
- the respective day of blood sampling. In short, the variable–diversity–joining (VDJ) rearranged
- 298 T-cell receptor beta (TRB) and immunoglobulin heavy (IGH) loci were amplified from 250-
- 299 500 ng genomic DNA in multiplex PCRs using the BIOMED2-FR1 (IGH) or –TRB-B primer
- 300 pools. Sequencing and demultiplexing was performed on an Illumina MiSeq sequencer (600-
- 301 cycle single-indexed, paired-end run, V3-chemistry). Read alignment was performed using the
- 302 MiXCR framework with the default reference library for TRB and the IMGT library v3 for IGH
- 303 (29). All nonproductive rearrangements and sequences with less than two read counts were not
- 304 included in downstream analyses. To correct for PCR bias, all IGH repertoires were
- proportionally normalized to 20,000, all TRB repertoires to 50,000 reads, respectively. A
- 306 clonotypes was defined as each unique complementarity-determining region 3 (CDR3)

- nucleotide sequence. Calculation of broad repertoire imprints and the VDJ architecture was performed using RStudio (version 1.1.456) as described (28, 30). Heatmaps were generated
- 309 using the R package *pheatmap*.
- 310 Human induced pluripotent stem cell (hiPSC) cardiomyocyte differentiation and
- 311 *maintenance*
- 312 HiPSC-cardiomyocytes were generated from a healthy iPSC line (31), maintained on Geltrex
- 313 coated 6-well plates using E8 full medium. Undifferentiated hiPSCs were seeded onto a
- 314 Geltrex-coated 12-well cell-culture dish with E8 full medium containing thiazovivin 3 days
- before start of differentiation. Differentiation was induced at day 0 when hiPSCs reached 70-
- 316 80% density. On day 0, the medium was shifted to Cardio Diff medium (RPMI
- 317 1640 + GlutaMAX, Thermo Fisher Scientific, #72400021) supplemented with human
- 318 recombinant albumin (Sigma-Aldrich, #A9731), L-Ascorbic acid 2-phosphate
- sesquimagnesium salt hydrate (Sigma-Aldrich, #A8960) and the GSK3β inhibitor CHIR99021
- 320 (5 μM). After 48 h, cells were supplemented with 5 mM of the Wnt signaling inhibitor IWP2
- 321 (Peprotech, #S7085) in fresh Cardio Diff media. Following medium changes were performed
- every 48 h. From day 8 on, cells were kept in Cardio Culture medium (RPMI 1640 + GlutaMAX
- supplemented with $1 \times B27$ with insulin, Thermo Fisher Scientific, #17504-001), with medium
- 324 changes every 2–3 days. HiPSC-cardiomyocytes were purified using metabolic selection and
- were used for 60-90 days after differentiation.
- 326 Time-dependent cell response profiling by real-time cell electronic sensing.
- The E96 xCELLigence plates (Agilent, USA) were coated with fibronectin (1:100 dilution in
- PBS, Promocell C-43050, 50 µL per well) with 1 h incubation at 37 °C. After equilibration to
- 329 37 °C, plates were inserted into the xCELLigence station (Agilent, USA), and the base-line
- 330 impedance was measured to ensure that all wells and connections were working within
- acceptable limits after removal of coating and addition of complete media (100 µL per well) as
- described (32). Following harvesting and counting, hiPSC-cardiomyocytes were diluted to
- seeding density of 30,000 cells per well ($100~\mu L$ per well) in Cardio Culture medium
- supplemented with thiazovivin and heat inactivated FBS. Two days after seeding, media change
- was performed every day (200 µL per well). On day 6 after seeding, 1% of respective patient
- serum was added to the wells while control wells were treated with 1% of Cardio Culture media.
- Three patient serotypes were tested including type 1) lowest levels for all identified AABs, 2)
- 338 highest levels for all identified AABs and 3) highest levels for all identified AABs but low
- levels for CXCR3ab. Contraction data was recorded every 24 h with 30 s sweeps. Beat rate and

amplitude at the 7th day after seeding was chosen for analysis and was calculated using the xCELLigence software.

Statistical analysis

342

343

344

345

346

347

348

349

350

351

352

353

354

355

356

357

358

359

360

361

362

363

Data was analyzed using SPSS (V.28, IBM, Armonk, USA) and GraphPad Prism (V.10, GraphPad Software, Boston, USA). Constant variables are expressed as mean \pm SD or 95% CI. Categorical variables are presented as n (%). Differences between groups were analyzed using one-factorial ANOVA or Kruskal-Wallis-Test (with Tukey's or Dunn's multiple comparisons test), and unpaired two-sided t-test or Mann-Whitney-U Test in case of non-normal distribution. Non-normal distribution was tested using skewness and kurtosis. Chi-square test was used for categorical variables. Spearman rank correlation analyses were performed to investigate correlations between AAB levels and HRV variables and ABB levels and time after acute infection and age. Trend lines for CPET-derived continuous parameters were modelled using asymmetrical third order polynomial curve fit with F statistics for comparison. In the discovery phase, a p-value < 0.15 was accepted as indicative of suggestive associations of sympathicus activation and ABB levels. Results of AIRR-seq were compared by overall AAB levels (seropositivity for ≥ 5 AABs vs. < 5 AABs) and by HFnu (low vs. high). Overall statistical significance was declared at p < 0.05. Logistic regression model was run using R (V.4.3.0) with HFnu as a binary outcome variable (0, low; 1, high). Predictor variables were standardized prior to modeling to ensure comparability in the logistic regression model. To assess the model's accuracy and mitigate the risk of overfitting, 10-fold cross-validation was used with each fold providing an accuracy score. The model's performance was evaluated using the area under the receiver operating characteristic (ROC) curve (AUC), sensitivity, and specificity. Feature importance was assessed by examining the absolute values of the regression coefficients for each predictor.

RESULTS

364

365

366

367

368

369

370

371

374

375

376

377

378

379

380

381

382

383

384

385

386

387

388

389

390

391

392

393

394

395

Pationts'	characteri	ictics
runems	CHUITUCIET	MUCH

PCS Patients (n=105; 42% women) were referred to rehabilitation with an average age of 49.3 \pm 11.4 years and a mean time interval between first infection and start of medical rehabilitation of 239 \pm 116 days. Fatigue/exercise intolerance and shortness of breath were observed in ~75% of patients with a mean Multidimensional Fatigue Inventory (MFI) score of 68.9 ± 14.4 (MFI cut-off value for chronic fatigue syndrome = 70 from 100). Cognitive dysfunction was less common (~59%). Sixteen patients (15.2%) had signs of tachycardia (resting heart rate > 100 bpm). During the acute phase of infection, ~70% of patients received ambulatory care or acute 372 care at home, while ~30% of patients required in-hospital care. Exercise capacity in terms of 373 peak oxygen uptake (peak VO₂) at admission was markedly reduced at $72.0 \pm 15.3 \%$ (17.8 + 4.0 ml·min⁻¹·kg⁻¹ VO₂), compared to reference (Table 1). Standard laboratory values were within reference, except for triglycerides, total cholesterol and LDL-cholesterol, for which the mean value was in the borderline-high range (Supplemental Table 2 of the Online Repository).

Discovery phase - Identification of suggestive anti-GPCR autoantibodies (GPCR-AABs)

To identify anti-GPCR AABs potentially associated with HRV alterations in PCS, 14 selected AABs with known targets contributing to PCS-specific symptoms were screened for differences between PCS patients with highest (top 20%, n=22) and lowest (lowest 20%, n=22) sympathicus activation determined by Holter ECG. As indicative parameter, HFnu over 24h was used (5). The comparison of AAB levels between the two groups suggested that 8 AABs including AGT1Rab, AGT2Rab, ADRB1ab, ADRB2ab, M1Rab, M3Rab, PAR1ab, and CXCR3ab may be associated with HRV alterations in PCS (Figure 1). The mean, minimal, and maximal levels of all tested AABs are given in Supplemental table 3 (of the Online Repository).

Immune repertoire architecture in PCS patients

Next, we profiled the peripheral B-cell receptor (BCR) and T-cell receptor (TCR) architecture by AIRR-seq to identify potential immunogenetic imprints of autoimmunity. To also test for potentially persisting SARS-CoV-2 signatures, we included immunogenic control data from COVID-19 patients with severe (n=26) or moderate (n=28) acute disease, after recovery (n=55)and pre-pandemic healthy individuals (n=59). All COVID-19 patients were sampled during the first wave of the pandemic when no vaccines were available. Patients' characteristics are given in Supplemental Table 1 of the Online Repository and have been described in detail elsewhere (33). Analysis of the broad BCR repertoire metrics revealed high similarity between PCS patients and healthy controls for clonality and diversity measures with a slight trend to higher richness in PCS (Figure 2A). The level of somatic hypermutation as proxy for antigenexperience was equal to healthy controls (Figure 2A). Compared to patients with moderate or severe COVID-19, PCS patients showed significantly lower BCR richness (p=0.0286 vs. moderate) and somatic hypermutation (p<0.0001 vs. severe) (Figure 2A). Principal component analysis (PCA) of IGHVJ gene usage showed a relatively homogenous overlapping gene architecture with the PCS samples, however, clustering denser on PC2 within the overlapping space (Figure 2B). This pattern was mainly driven by a higher frequency of B cells with IGHV4-39 and IGHV4-59 rearrangements in PCS (Figure 2C). Notably, IGHV4-39 and IGHV4-59 genes have been described in several settings of autoimmunity including rheumatoid factors and antiphospholipid syndrome (34, 35). Subsetting PCS patients for autoantibody positivity (≥5 AABs above group median) or HFnu values did not reveal clear patterns with respect to repertoire metrics or IGHV gene usage (Figure 2D+E). However, we observed small trends for higher richness and Simpson diversity in HFnu high as compared to the HFnu low (Figure 2D) and a small trend for higher clonality and IGHV4-59 usage in patients with less than 5 positive AAB species (Figure 2E). Notably, we did not observe increased usage of IGHV3-30 or IGHV3-30-3 rearrangements as reported for ME/CFS (36). Similar to BCR metrics, the TCR repertoires of PCS patients did not display differences to healthy individuals with respect to richness, clonality and diversity indices (Figure 2F). Compared to patients with moderate or severe COVID-19 or recovered patients, PCS patients showed significantly altered TCR richness (p=0.0008 vs. severe; p <0.0001 vs. recovered), and lower diversity indices (Shannon, p= 0.0002, Simpson, p <0.0001 vs. recovered) (Figure 2F). No overall differences for PCS patients in terms of global VJ architecture was detected (Figure 2G). However, PCS patients displayed slightly increased frequencies of T-cell receptor beta variable (TRBV)29-1 and TRBV6-5 rearrangements and slightly decreased frequencies of TRBV27 and TRBV11-3 rearrangements (Figure 2H). Except for a slight decrease of Simpson diversity in PCS patients with low HFnu values and a trend towards higher clonality in PCS patients with less than 5 AAB species, we did not observe any differences in repertoire metrics or TRBV gene usage in HFnu and AAB cohort subsets (Figure 2I+J).

In-depths analysis of identified anti-GPCR AABs

426 General observations

396

397

398

399

400

401

402

403

404

405

406

407

408

409

410

411

412

413

414

415

416

417

418

419

420

421

422

423

424

425

- The levels of 8 suggestive anti-GPCR AABs were determined in the entire cohort of PCA
- patients (n=105). Comparison with reference values indicated seroprevalence at 14.3% for

- AGT1Rab, 5.7% for AGT2Rab, 42.9% for ADRB1ab, 53.3% for ADRB2ab, 29.5% for M1Rab, 429 49.5% for M3Rab, 41.0% PAR1ab, and 17.1 % for CXCR3ab (Supplemental table 3 of the 430 Online Repository). While AABs levels were comparable between women and men (all p \geq 431 0.133), some correlations with age were observed in that significantly lower levels of 432 AGT1Rab, ADRB1ab, and ADRB2ab were detected in older patients ($p \le 0.0174$, $r \le -0.24$) 433 (Supplemental figure 2 of the Online Repository). None of the tested AABs affected the PCS 434 patients' relative physical performance assessed by CPET at the time of admission. Of note, a 435 general trend to lower AAB levels with in-hospital acute care was observed which was 436 significant for AGT1Rab, ADRB1ab, and ADRB2ab (ambulant vs. in-hospital care without 437 ventilation, $p \le 0.0278$), while highest level for CXCR3ab were detected in patients with 438 ventilation (p = 0.0009 vs. ambulant care) (Figure 3A). However, no specific treatment 439 (antiviral, anti-inflammatory) was identified that could explain this observation. Most of the 440 tested AABs showed no association with time after acute infection (all p > 0.05), but levels of 441 CXCR3ab were highest in patients with a more recent SARS-CoV-2 infection (r = -0.349, 442 443 p=0.0003) (Figure 3B). Elevated AAB levels showed significant intra-individual correlations in that ADRB1ab and ADRB2ab correlated at r = 0.96 (p<0.0001) and levels of ADRB1/2ab 444 correlated strongly with AGT1Rab and M3Rab (all $r \ge 0.823$, p < 0.0001) but at a lower level 445 with CXCR3ab (r = 0.308, p = 0.001) (Supplemental figure 3). 446
- 447 Predictive modeling of sympathicus activation based on anti-GPCR AABs
- 448 To analyze which of the suggestive anti-GPCR AABs has the highest standardized impact on sympathicus activation and at what level of accuracy sympathicus activation can be predicted 449 based on AABs, a logistic regression model was built based on the 8 identified AABs and HFnu 450 as binary outcome (Figure 4). The logistic regression model achieved a mean 10-fold cross-451 validated accuracy of $67.5\% \pm 11.5\%$, indicating reasonable performance, with some variability 452 across the folds. When evaluated on the full dataset, the model's AUC was 0.78, indicating 453 moderate discriminative power with a balanced trade-off between sensitivity and specificity. A 454 455 confusion matrix was used to show that the model correctly identified 42 cases (81%) as class 0 (HFnu low) and 33 cases (67%) in class 1 (HFnu high). Feature importance analysis revealed 456 that CXCR3Ab had the highest impact on the outcome (27.7%), followed by M3Rab (20.2%) 457 and M1Rab (15.0%) (Figure 4). 458

Anti-GPCR AAB associations with HRV variables

459

To investigate the effect of the identified AABs on different autonomic nervous system functions, HRV variables including frequency domain variables, time domain variables, and

nonlinear variables (as defined by the analysis of Poincaré maps) were analyzed for their association with AAB levels (Table 2). The results suggested that time-related variables rMSSD and pNN50 were mainly affected by AGT1Rab, ADRB1/2ab, and M3Rab during day and night periods and over the entire recording time of 24h in that higher AAB levels were associated with higher rMSSD and pNN50 values (p≤0.022). M1Rab, CXCR3ab and PAR1ab had no effect on time-related HRV variables. A comparable pattern was observed for non-linear HRV variables, where again M1Rab, CXCR3ab and PAR1ab had no effect but AGT1Rab, ADRB1/2ab, and M3Rab showed low-to-moderate positive effects on variables SD1 and VAI (p≤0.019). In terms of frequency-related variables, a different pattern was observed in that CXCR3ab had opposing effects to AGT1Rab, ADRB1/2ab, and M3Rab. While AGT1Rab, ADRB1/2ab, and M3Rab had positive effects on HF power and HFnu (24h period, p≤0.036) and overall normalized parasympathetic activity (6h day, 6h night, and 24h period), CXCR3ab levels had negative effects on HF power and HFnu (6h day and 24h period; p≤0.041) and negative effects on overall normalized parasympathetic activity (6h night, and 24h period; p≤0.037). Of note, CXCR3ab increased the ratio between LF and HF over the 24h period and over the 6h night period (p=0.037), which is of relevance since a higher LF/HF ratio indicates a dominating sympathetic system (Table 2).

Vasoactivity of anti-GPCR AABs

To investigate the overall cardio- and vasoactive effects of the identified anti-GPCR AABs with the most prominent influence on sympathetic and parasympathetic activity (Table 2), we tested whether AABs affected BP and HR using 24h BP measurement. Results indicated that high levels of CXCR3ab were linked to higher mean arterial pressure (MAP) during the day and night period as well as over the entire measurement period of 24h (both p ≤ 0.046) (Figure 5A), while BP appeared unaffected by the other tested AABs (Supplemental figure 4). A mean 24h MAP above the threshold of 105 mmHg was detected in 22% of patients with high CXCR3ab levels but only in 11% of patients with low CXCR3ab levels. This finding was supported by analysis of medication which indicated that prescription rates of BP medication were higher in PCS patients with high CXCR3ab levels compared to patients with low CXCR3ab levels (77% vs. 51%, p=0.023). Since no effect on 24h HR values was seen for any AAB (Supplemental figure 4), we tested if AAB levels against ADRB1 would affect the HR response under controlled conditions (i.e. standardized CPET) and whether intake of beta blockers interfered with this response. This analysis revealed that PCS patients receiving beta blockers showed a clear reduction in HR increase and peak HR during exercise testing compared to patients

without beta blockers (p <0.05) (Figure 5B). Moreover, ADRB1ab levels did not show any effect on HR response during exercise testing, neither in patients with nor without beta blockers (Figure 4). The influence of AABs on BP response and blood oxygen saturation (SPO₂) during CPET was also tested. In terms of BP response, patients with higher levels of AGT1Rab had an increased diastolic blood pressure (DBP) response during CPET compared to patients with lower AGT1Rab levels (p<0.001). In terms of elevated M1Rab and CXCR3ab levels, patients showed higher DBP and MAP values during CPET compared to patients with lower levels (p≤0.035). In addition, patients with higher CXCR3ab levels also showed reduced SPO₂ during exercise testing (p<0.027).

In vitro effects of anti-GPCR AABs

Finally, we tested whether the anti-GPCR AABs had a direct effect on the electromechanical coupling of cardiac myocytes using time-dependent *in vitro* cell response profiling by real-time cell electronic sensing. Using human induced pluripotent stem cell (hiPSC) derived cardiomyocytes we analyzed the serum effects on cardiomyocyte contraction profiles (Figure 6). Results indicated that a general effect of patient serum on the cell contractility (beats per minute) existed, which was however independent of patients' serotype (Figure 6C), making a specific effect of AABs on beat frequence unlikely. Likewise, AABs had no effect on the amplitude of cardiomyocyte contraction (Figure 6D).

DISCUSSION

514

515

516

517

518

519

520

521

522

523

524

525

526

527

528

529

530

531

532

533

534

535

536

537

538

539

540

541

542

543

544

545

546

This study investigated the regulatory capacity of anti-GPCR AABs targeting central components of the autonomic nervous system and pivotal vasoregulatory and inflammatory receptors in patients with long-term Post-COVID-19 Syndrome (PCS). Using heart rate variability (HRV) as well as 24h and exercise blood pressure analysis combined with analysis of immunogenetic imprints of autoimmunity and in vitro analyses of AAB effects on electromechanical coupling in stem cell-derived cardiomyocytes we found that (1) anti-GPCR AABs detected in PCS patients affect the autonomic nervous system as indicated by altered rhythm control and vasoregulation, (2) AABs against CXCR3, M1/M3, AGTR1 and ADRB1/2 showed partly opposite effects on HRV parameters suggesting dysfunctional regulation of the autonomic nervous system (3) AABs against the CXCR3 receptor may prevent parasympathetic activation in PCS patients mainly at night, (4) PCS patients with high AAB levels against AGTR1, M1 and CXCR3 showed elevated stress-induced blood pressure responses, (5) AAB levels and HFnu values did not correlated with B- and T-cell receptor repertoire metrics or TRBV gene usage, and finally, (6) serum AAB targeting GPCR did not affect contractility of stem cell derived cardiac myocytes suggesting a more systemic action of AABs. To the best of our knowledge, this study is the first to describe that anti-parasympathetic and anti-adrenergic AABs as well as AABs against the T-cell receptor CXCR3 are linked to autonomic dysfunction and vasoregulation in patients with PCS. So far, several studies have investigated the role of immunological dysregulation and AABs in patients with PCS aiming at a better understanding of the condition and related symptoms as well as the development of diagnostic tools and potential therapeutic interventions (37-40). Based on the concept that a SARS-CoV-2 infection may induce an ongoing activation of the immune system, e.g. due to an ineffective virus elimination, a trigger of autoimmune processes may occur. AABs against different factors in distinct pathways and AABs identified in autoimmune diseases have been investigated in PCS patients' serum or plasma. This included AABs specific to rheumatoid diseases and central components of the immune system, thyroidrelated AABs as well as AABs against components of the cardiovascular system, among others (18, 39-42). While autoimmunity during acute COVID-19 is mirrored by peripheral repertoire imprints (43,44), we did not observe similar patterns in our PCS cohort, despite serological positivity. A possible reason for this discrepancy is that the systemic hyperinflammation during acute COVID-19 may lower tolerance thresholds for inherently autoreactive lymphocytes resulting in characteristic repertoire imprints (28,43,44), while (de novo) autoreactivity in PCS may be rather elicited by persisting local antigenic reservoirs (45). Notably, we also did not observe BCR signatures reported for ME/CFS (36) supporting an etiological distinction of both syndromes.

550

551

552

553

554

555

556

557

558559

560

561

562

563

564

565

566

567

568

569

570

571

572

573

574

575

576

577

578

579

580

Irrespective of a definitive molecular driver, recent comprehensive reviews have acknowledged that a variety of AABs can occur after a SARS-CoV-2 infection some of which can be persistent and may potentially contribute to signs and symptoms observed in PCS (39,40). The systematic analysis by Notare et al. concluded that there is evidence for a potential association between the presence of AABs and PCS and that the presence of AABs may contribute to the ongoing inflammation and multisystemic manifestations of the condition (40). Moreover, the presence of AABs correlated with clinical symptoms and levels of AABs were higher in patients with PCS compared to those not developing PCS after a SARS-CoV-2 infection (46-48). Notably, increased ADRB2 AAB levels were associated with the severity of vasomotor symptoms in PCS (18). Using HRV as an objective measure of the autonomic nervous system we and others have recently detected autonomic imbalance in patients with PCS (low parasympathetic tone, enhanced sympathetic tone) (5, 49). In the current study, we provide evidence that autonomic imbalance is related to an anti-GPCR AAB pattern. Our findings indicate that AABs against ADRB1/2, AGTR1, M1/M3, and CXCR3 have partly opposing effects on HRV variables. Time-related variables such as rMSSD and pNN50 were predominantly correlated to AGT1Rab, ADRB1/2ab, and M3Rab levels. Similarly, these AABs affected HF power, an indicator of parasympathetic activity, within the frequency related variables. In contrast, CXCR3ab levels were inversely correlated with HF power and HFnu and were associated with an enhanced LF/HF ratio over the 24h period, indicating an overall dominating sympathetic system in PCS patients with high CXCR3ab levels. Such an inverse correlation between parasympathetic activity and pro-inflammatory status has been described in other chronic inflammatory diseases such inflammatory bowel disease and rheumatic arthritis (50). The finding that the generated linear regression model identified CXCR3ab together with M3Rab with the highest standardized impact on HFnu, suggests that the detected positive effects of AGT1Rab and ADRB1/2ab might be hampered. This further points to a complex interplay of AABs against G-protein coupled receptors with either stimulatory or non-stimulatory function potentially competing with natural ligands. Our findings did not indicate a direct effect of the investigated AABs on HR, neither during 24h monitoring nor during controlled exercise stress tests. This was in line with in vitro experiments on serum-dependent changes in contractility of hiPSC-derived cardiomyocytes, suggesting that the myocardial cell itself may not be the target of GPCR AABs pointing towards a more systemic action. To this extend, AABs have been

581

582

583

584

585

586

587

588

589

590

591

592

593

594

595

596

597

598

599

600

601

602

603

604

605

606

607

608

609

610

611

612

613

linked to autonomic neuropathy and there is evidence for persistent inflammation and prolonged NETosis several months after an acute COVID-19 infection (51). NET release enables self-antigen exposure and AAB production, thereby increasing the autoinflammatory response with nerval damage (52). Similarly to the recently described peripheral autonomic neuropathy (53), cardiac autonomic neuropathy may therefore be proposed to contribute to altered HRV.

Persistent inflammation during PCS might also explain the observed levels of CXCR3abs. Ryan et al. demonstrated an enhanced CXCR3 receptor expression on cells of the innate immune system such as neutrophils and monocytes several months after an acute COVID-19 infection using deep immunophenotyping (54). Moreover, a direct link between activation of the sympathetic nervous system and CXCR3 has been suggested in that acute stress leading to induced sympathetic cardiac activation, parasympathetic cardiac withdrawal, lymphocytosis has been shown to increase the number of circulating T cells expressing CXCR3 (55). In addition, CXCR3ab levels appear to be associated with COVID-19 severity, since CXCR3ab levels were highest in patients with need for ventilation during the acute SARS-CoV-2 infection, a finding in line with a previous report that AAB levels against CXCR3 depend on the severity of the acute COVID-19 infection (22). It thus seems conceivable that both an overactivation of the sympathetic nervous system and ongoing autoimmune activity during the acute SARS-CoV-2 infection (13) may lead to elevated levels of AABs against CXCR3. This is of relevance since CXCR3 may be linked to different signs and symptoms seen in PCS. CXCR3 is expressed on several cell types of the central nervous system and cardiovascular system and has been implicated in several central nervous system disorders, likely based on the observation that CXCR3-expressing T cells infiltrate the central nervous system, and binding of chemokine IP-10 (interferon-inducible protein of 10 kDa) to CXCR3 expressing cells leads to apoptosis of neurons and subsequent neuronal damage (56). To this end, Blank et al. (57) found that Mice lacking IP-10 or Cxcr3 were protected from depressive behavior and impaired learning and memory. The authors suggested that brain endothelial and epithelial cells play an important role in communication between the central nervous system and the immune system and that the brain endothelial IFNAR-IP-10 axis modulates cognitive impairment and sickness behavior in a CXCR3-dependent manner.

CXCR3 may also be linked to vascular changes in terms of atherosclerosis as well as hypertension since CXCR3 ligands have been shown to be increased in patients with essential hypertension (58). In addition, IP-10-mediated inhibition of endothelial cell migration via proteoglycan signalling and angiostatic actions of the IP-10-CXCR3 axis has been described

(58, 59). While we cannot directly conclude on the functional activity of the CXCR3abs 614 detected in the involved PCS patients, an agonistic activity of AABs at CXCR3 with IP-10 615 mimicking function could explain our observation of higher MAP and stress-induced BP 616 response in patients with higher CXCR3ab levels. To what extend BP elevations in PCS may 617 depend on initially elevated transient levels of CXCR3abs during the acute COVID-19 infection 618 and subsequent changes in endothelial function and inhibition of angiogenesis and suppression 619 of new blood vessel growth needs to be analyzed further. These CXCR3ab effects may however 620 621 provide at least a partial explanation for the described endothelial and microvascular alterations in PCS (8, 60-62). 622 In terms of AABs against M1R and M3R it needs to be stated that whether muscarinic receptors 623 play a crucial role in regulating HR or BP in humans remains unclear even though muscarinic 624 receptors regulate key functions in the central and peripheral nervous systems (63). M1R 625 stimulation in the sympathetic ganglia of laboratory animals has been shown to induce 626 norepinephrine release from sympathetic terminals resulting in vasoconstriction. Studies in 627 628 humans suggest that M3R is responsible for endothelial-mediated vasodilation induced by exogenous acetylcholine. Because cholinergic innervation of human blood vessels is almost 629 nonexistent, it is unclear how acetylcholine-mediated endothelial function occurs in 630 physiological conditions (63). Together with the observed effects of higher M1Rab levels on 631 stress-induced BP, it may be postulated that AABs against M1R function as M1R agonists 632 633 stimulating norepinephrine release resulting in vasoconstriction. Future work should aim at understanding whether the seroprevalence of the here described 634 AABs varies depending on the different SARS-CoV-2 lineages and whether (recurrent) 635 vaccination may reduce the risk of the emergence of AABs based on reports that vaccinated 636 individuals may be at lower risk of developing PCS and potentially reduce inflammation and 637 symptom burden when vaccinated post-PCS diagnosis (64, 65). Also, processes underlying 638 AAB production in PCS in general, and the role of B cell activation and CXCR3-positive T 639 cells in particular, need to be investigated further (16). To what extent therapeutic apheresis is 640 capable to reduce AABs and disease burden is currently not clear. Preliminary evidence 641 suggests that apheresis may reduce ADRB1/2abs by ~30% and M3Rab by ~50% and patients 642 showing a significant reduction in these AABs together with inflammatory markers reported 643 significant symptom improvement after two cycles of apheresis (66). Further studies in the field 644 of IgG depletion by immunoadsorption are currently being conducted to identify which patients 645 may benefit from the procedure (67). Most recently, a placebo-controlled phase IIa clinical trial 646

of rovunaptabin (BC007) showed a neutralizing effect on anti-GPCR AABs and an associated improvement of symptoms in PCS. It needs to be investigated if BC007 also neutralizes the here identified AABs and if the aptamer can effectively restore the associated anti-parasympathetic and anti-adrenergic activities (68).

Limitations

The findings of this study may be limited since the analyzed cohort was recruited from patients participating in exercise-based rehabilitation. Thus, patients with more severe PCS which are unable to participate in an active rehabilitation program were not included. The determined AAB levels were interpreted based on laboratory reference values and no direct control group was involved. Also, we did not obtain AAB levels prior to SARS-CoV-2 infection and cannot account for patients who may have had an undocumented underlying autoimmune disease or other factors contributing to AAB levels. Also, the number of exposures to different SARS-CoV-2 variants as well as the number of undiagnosed (repeated) COVID-19 infections and the timing of immunization might have affected the outcome.

CONCLUSION

We conclude that anti-parasympathetic and anti-adrenergic AABs are associated with autonomic dysfunction and disturbed vasoregulation in patients with PCS. AABs against Gai protein-coupled receptor CXCR3 are inversely related to parasympathetic tone thereby leading to an overall dominating activity of the sympathetic system. Moreover, PCS patients with elevated CXCR3ab and M1Rab levels show an increased stress-induced blood pressure elevation. The investigated AAB levels did not correlate with B- and T-cell receptor repertoire metrics or TRBV gene usage and BCR signatures differed from those reported for ME/CFS patients. A direct effect of the investigated AABs on electromechanical coupling of stem cell-derived cardiac myocytes *in vitro* was not confirmed. Taken together, these findings suggest that AABs targeting GPCRs play a modulatory role in sympathetic nervous system-mediated regulation of both cardiac rhythm and vascular function in PCS.

673	Author contributions
674	Concept and design: BS, FCM; Patient recruitment and clinical investigation: FCM, RG;
675	Measurement of antibodies: HH; Adaptive immune receptor repertoire sequencing: CS, MB;
676	Human induced pluripotent stem cell (HiPSC) cardiomyocyte differentiation and in vitro
677	electromechanical coupling: CB, SC; Clinical data acquisition: RG, HS; Data Processing: RG,
678	HS, BS; Statistical analysis: BS, CS; Drafting the article: BS, FCM; Critical revision: HH, GR;
679	All authors approval of the final version.
680	Data availability
681	Datasets used in this study are available from the corresponding author upon reasonable request.
682	Funding
683	FCM and BS are supported by the European Commission within the Horizon 2020 framework
684	program (grant number: 101017424). MB is supported by the German Research Foundation
685	(award SFB 1648/1 2024-512741711). Support for CB and SC was endorsed by the COVID-
686	19 Research Network Lower Saxony (COFONI).
687	Competing interests
688	BS has received speaker honoraria from Biotronik unrelated to this work. KSF and HH are co-
689	founders of CellTrend GmbH. All other authors declare no competing interests.
690	Additional information
691	Correspondence and requests for materials should be addressed to FCM.
692	
693	

694 **REFERENCES**

- Koczulla AR, Ankermann T, Behrends U, Berlit P, Berner R, Böing S, et al. S1-Leitlinie
 Long-/Post-COVID [German S1 Guideline Long-/Post-COVID]. Pneumologie.
 2022;76(12):855-907. doi:10.1055/a-1946-3230
- Oronsky B, Larson C, Hammond TC, Oronsky A, Kesari S, Lybeck M, et al. A review of persistent post-COVID syndrome (PPCS). Clin Rev Allergy Immunol. 2023;64(1):66-74.
- Nalbandian A, Sehgal K, Gupta A, Madhavan MV, McGroder C, Stevens JS, et al. Post-acute COVID-19 syndrome. Nat Med. 2021;27(4):601-15.
- Soriano JB, Murthy S, Marshall JC, Relan P, Diaz JV. A clinical case definition of post COVID-19 condition by a Delphi consensus. Lancet Infect Dis. 2022;22(4):e102-e107.
- Mooren FC, Böckelmann I, Waranski M, Kotewitsch M, Teschler M, Schäfer H, et al. Autonomic dysregulation in long-term patients suffering from post-COVID-19 syndrome assessed by heart rate variability. Sci Rep. 2023;13(1):15814. doi:10.1038/s41598-023-42615-y
- Garbsch R, Schäfer H, Kotewitsch M, Mooren JM, Waranski M, Teschler M, et al. Sex specific differences of cardiopulmonary fitness and pulmonary function in exercise based rehabilitation of patients with long-term post-COVID-19 syndrome. BMC Med.
 2024;22(1):446. doi:10.1186/s12916-024-03658-8
- 713 7. Serviente C, Decker ST, Layec G. From heart to muscle: pathophysiological mechanisms underlying long-term physical sequelae from SARS-CoV-2 infection. J Appl Physiol (1985). 2022;132(3):581-92.
- Schäfer H, Teschler M, Mooren FC, Schmitz B. Altered tissue oxygenation in patients with post COVID-19 syndrome. Microvasc Res. 2023;148:104551.
- 718 9. Appelman B, Charlton BT, Goulding RP, Kerkhoff TJ, Breedveld EA, Noort W, et al.
 719 Muscle abnormalities worsen after post-exertional malaise in long COVID. Nat
 720 Commun. 2024;15:17. doi:10.1038/s41467-023-44432-3
- 721 10. Mingoti MED, Bertollo AG, Simões JLB, Francisco GR, Bagatini MD, Ignácio ZM.
 722 COVID-19, oxidative stress, and neuroinflammation in the depression route. J Mol
 723 Neurosci. 2022;72(6):1166-81.
- 11. Al-Kuraishy HM, Al-Gareeb AI, Qusti S, Alshammari EM, Gyebi GA, Batiha GE. COVID-19-induced dysautonomia: a menace of sympathetic storm. ASN Neuro. 2021;13:17590914211057635. doi:10.1177/17590914211057635
- Jamal SM, Landers DB, Hollenberg SM, Turi ZG, Glotzer TV, Tancredi J., et al.
 Prospective evaluation of autonomic dysfunction in post-acute sequela of COVID-19. J
 Am Coll Cardiol. 2022;79:2325-30. doi:10.1016/j.jacc.2022.03.357
- 730 13. Scala I, Rizzo PA, Bellavia S, Brunetti V, Colò F, Broccolini A, et al. Autonomic dysfunction during acute SARS-CoV-2 infection: a systematic review. J Clin Med. 2022;11:3883. doi:10.3390/jcm11133883
- Li J, Kong X, Liu T, Xian M, Wei J. The role of ACE2 in neurological disorders: from underlying mechanisms to the neurological impact of COVID-19. Int J Mol Sci. 2024;25(18):9960. doi:10.3390/ijms25189960
- Bielecka E, Sielatycki P, Pietraszko P, Zapora-Kurel A, Zbroch E. Elevated arterial blood pressure as a delayed complication following COVID-19—a narrative review. Int
 J Mol Sci. 2024;25(3):1837. doi:10.3390/jims25031837
- Tsay GJ, Zouali M. Cellular pathways and molecular events that shape autoantibody production in COVID-19. J Autoimmun. 2024;147:103276. doi:10.1016/j.jaut.2024.103276

- 742 17. Notarte KI, Carandang THDC, Velasco JV, Pastrana A, Ver AT, Manalo GN, et al. 743 Autoantibodies in COVID-19 survivors with post-COVID symptoms: a systematic 744 review. Front Immunol. 2024;15:1428645. doi:10.3389/fimmu.2024.1428645
- 745 18. Sotzny F, Filgueiras IS, Kedor C, Freitag H, Wittke K, Bauer S, et al. Dysregulated 746 autoantibodies targeting vaso- and immunoregulatory receptors in post COVID 747 syndrome correlate with symptom severity. Front Immunol. 2022;13:981532. 748 doi:10.3389/fimmu.2022.981532
- 749 19. Bastard P, Rosen LB, Zhang Q, Michailidis E, Hoffmann HH, Zhang Y, et al.
 750 Autoantibodies against type I IFNs in patients with life-threatening COVID-19.
 751 Science. 2020;370(6515):eabd4585. doi:10.1126/science.abd4585
- Zuo Y, Estes SK, Ali RA, Gandhi AA, Yalavarthi S, Shi H, et al. Prothrombotic autoantibodies in serum from patients hospitalized with COVID-19. Sci Transl Med. 2020;12(570):eabd3876. doi:10.1126/scitranslmed.abd3876
- 755 21. Rodriguez-Perez AI, Labandeira CM, Pedrosa MA, Valenzuela R, Suarez-Quintanilla JA, Cortes-Ayaso M, et al. Autoantibodies against ACE2 and angiotensin type-1 receptors increase severity of COVID-19. J Autoimmun. 2021;122:102683. doi:10.1016/j.jaut.2021.102683
- Cabral-Marques O, Halpert G, Schimke LF, Ostrinski Y, Vojdani A, Baiocchi GC, et
 al. Autoantibodies targeting GPCRs and RAS-related molecules associate with COVID severity. Nat Commun. 2022;13(1):1220. doi:10.1038/s41467-022-28905-5
- Cabral-Marques O, Marques A, Giil LM, De Vito R, Rademacher J, Günther J, et al. GPCR-specific autoantibody signatures are associated with physiological and pathological immune homeostasis. Nat Commun. 2018;9(1):5224. doi:10.1038/s41467-018-07598-9
- Loebel M, Grabowski P, Heidecke H, Bauer S, Hanitsch LG, Wittke K, et al. Antibodies
 to beta-adrenergic and muscarinic cholinergic receptors in patients with chronic fatigue
 syndrome. Brain Behav Immun. 2016;52:32-9. doi:10.1016/j.bbi.2015.09.013
- Reinshagen L, Nageswaran V, Heidecke H, Schulze-Forster K, Wilde AB, Ramezani
 Rad P, et al. Protease-activated receptor-1 IgG autoantibodies in patients with COVID Thromb Haemost. 2024;124(12):1164-6. doi:10.1055/a-2205-0014
- Task Force of the European Society of Cardiology and the North American Society of Pacing and Electrophysiology. Heart rate variability: standards of measurement, physiological interpretation and clinical use. Circulation. 1996;93(5):1043-65.
- 775 27. Mooren JM, Garbsch R, Schäfer H, Kotewitsch M, Waranski M, Teschler M, et al. Medical rehabilitation of patients with post-COVID-19 syndrome—a comparison of aerobic interval and continuous training. J Clin Med. 2023;12(21):6739.
- Schultheiß C, Paschold L, Mohebiany AN, Escher M, Kattimani YM, Müller M, et al.
 A20 haploinsufficiency disturbs immune homeostasis and drives the transformation of lymphocytes with permissive antigen receptors. Sci Adv. 2024;10(34):eadl3975.
 doi:10.1126/sciadv.adl3975
- 782 29. Bolotin DA, Poslavsky S, Mitrophanov I, Shugay M, Mamedov IZ, Putintseva EV, et al. MiXCR: software for comprehensive adaptive immunity profiling. Nat Methods. 2015;12(5):380-1. doi:10.1038/nmeth.3364
- Simnica D, Schliffke S, Schultheiß C, Bonzanni N, Fanchi LF, Akyüz N, et al. Highthroughput immunogenetics reveals a lack of physiological T-cell clusters in patients with autoimmune cytopenias. Front Immunol. 2019;10:1897. doi:10.3389/fimmu.2019.01897
- Haase A, Gohring G, Martin U. Generation of non-transgenic iPS cells from human cord blood CD34(+) cells under animal component-free conditions. Stem Cell Res. 2017;21:71-3.

- 792 32. Mewes M, Lenders M, Stappers F, Scharnetzki D, Nedele J, Fels J, et al. Soluble 793 adenylyl cyclase (sAC) regulates calcium signaling in the vascular endothelium. 794 FASEB J. 2019;33(12):13762-74. doi:10.1096/fj.201900724R
- 795 33. Schultheiß C, Paschold L, Simnica D, Mohme M, Willscher E, von Wenserski L, et al. Next-generation sequencing of T- and B-cell receptor repertoires from COVID-19 patients showed signatures associated with severity of disease. Immunity. 2020;53(2):442-455.e4. doi:10.1016/j.immuni.2020.06.024
- Zhou S, Liu Z, Yuan H, Zhao X, Zou Y, Zheng J, et al. Autoreactive B-cell differentiation in diffuse ectopic lymphoid-like structures of inflamed pemphigus lesions. J Invest Dermatol. 2020;140(2):309-318.e8. doi:10.1016/j.jid.2019.07.717
- Bende RJ, Janssen J, Wormhoudt TA, Wagner K, Guikema JE, van Noesel CJ. Identification of a novel stereotypic IGHV4-59/IGHJ5-encoded B-cell receptor subset expressed by various B-cell lymphomas with high-affinity rheumatoid factor activity. Haematologica. 2016;101(5):e200-e203. doi:10.3324/haematol.2015.139626
- Sato W, Ono H, Matsutani T, Nakamura M, Shin I, Amano K, et al. Skewing of the Bcell receptor repertoire in myalgic encephalomyelitis/chronic fatigue syndrome. Brain Behav Immun. 2021;95:245-55. doi:10.1016/j.bbi.2021.03.023
- Saito S, Shahbaz S, Osman M, Redmond D, Bozorgmehr N, Rosychuk RJ, et al. Diverse immunological dysregulation, chronic inflammation, and impaired erythropoiesis in long COVID patients with chronic fatigue syndrome. J Autoimmun. 2024;147:103267. doi:10.1016/j.jaut.2024.103267
- Tsay GJ, Zouali M. Cellular pathways and molecular events that shape autoantibody production in COVID-19. J Autoimmun. 2024;147:103276. doi:10.1016/j.jaut.2024.103276
- Dobrowolska K, Zarębska-Michaluk D, Poniedziałek B, Jaroszewicz J, Flisiak R, Rzymski P. Overview of autoantibodies in COVID-19 convalescents. J Med Virol. 2023;95(6):e28864. doi:10.1002/jmv.28864
- Notarte KI, Carandang THDC, Velasco JV, Pastrana A, Ver AT, Manalo GN, et al. Autoantibodies in COVID-19 survivors with post-COVID symptoms: a systematic review. Front Immunol. 2024;15:1428645. doi:10.3389/fimmu.2024.1428645
- Epstein-Shuman A, Hunt JH, Caturegli P, Winguth P, Fernandez RE, Rozek GM, et al. Autoantibodies directed against interferon alpha, nuclear antigens, cardiolipin, and beta-2 glycoprotein 1 are not induced by SARS-CoV-2 or associated with long COVID. Int J Infect Dis. 2024 Nov 1:107289. doi:10.1016/j.ijid.2024.107289
- Matula Z, Király V, Bekő G, Gönczi M, Zóka A, Steinhauser R, et al. High prevalence of long COVID in anti-TPO positive euthyroid individuals with strongly elevated SARS-CoV-2-specific T-cell responses and moderately raised anti-spike IgG levels 23 months post-infection. Front Immunol. 2024;15:1448659. doi:10.3389/fimmu.2024.1448659
- Woodruff MC, Ramonell RP, Nguyen DC, Cashman KS, Saini AS, Haddad NS, et al. Extrafollicular B-cell responses correlate with neutralizing antibodies and morbidity in COVID-19. Nat Immunol. 2020;21(12):1506-16. doi:10.1038/s41590-020-00814-z
- Schultheiß C, Paschold L, Willscher E, Simnica D, Wöstemeier A, Muscate F, et al. Maturation trajectories and transcriptional landscape of plasmablasts and autoreactive B cells in COVID-19. iScience. 2021;24(11):103325. doi:10.1016/j.isci.2021.103325
- Proal AD, VanElzakker MB, Aleman S, Bach K, Boribong BP, Buggert M, et al. SARS CoV-2 reservoir in post-acute sequelae of COVID-19 (PASC). Nat Immunol.
 2023;24(10):1616-27. doi:10.1038/s41590-023-01601-2
- Seibert FS, Stervbo U, Wiemers L, Skrzypczyk S, Hogeweg M, Bertram S, et al. Severity of neurological long-COVID symptoms correlates with increased level of

- autoantibodies targeting vasoregulatory and autonomic nervous system receptors.

 Autoimmun Rev. 2023;22:103445. doi:10.1016/j.autrev.2023.103445
- Son K, Jamil R, Chowdhury A, Mukherjee M, Venegas C, Miyasaki K, et al. Circulating anti-nuclear autoantibodies in COVID-19 survivors predict long-COVID symptoms. Eur Respir J. 2022;61:2200970. doi:10.1183/13993003.00970-2022
- 48. L'Huillier AG, Pagano S, Baggio S, Meyer B, Andrey DO, Nehme M, et al.
 Autoantibodies against apolipoprotein A-1 after COVID-19 predict symptoms
 persistence. Eur J Clin Invest. 2022;52:e13818. doi:10.1111/eci.13818
- 49. Fedorowski A, Fanciulli A, Raj SR, Sheldon R, Shibao CA, Sutton R. Cardiovascular
 autonomic dysfunction in post-COVID-19 syndrome: a major health-care burden. Nat
 Rev Cardiol. 2024;21(6):379-95. doi:10.1038/s41569-023-00962-3
- Dotan I. New serologic markers for inflammatory bowel disease diagnosis. Dig Dis. 2010;28(3):418-23. doi:10.1159/000320396
- Ng H, Havervall S, Rosell A, Aguilera K, Parv K, von Meijenfeldt FA, et al. Circulating markers of neutrophil extracellular traps are of prognostic value in patients with COVID-19. Arterioscler Thromb Vasc Biol. 2021;41(2):988-94. doi:10.1161/ATVBAHA.120.315267
- Dotan A, Muller S, Kanduc D, David P, Halpert G, Shoenfeld Y. The SARS-CoV-2 as an instrumental trigger of autoimmunity. Autoimmun Rev. 2021;20(4):102792. doi:10.1016/j.autrev.2021.102792
- Maguire C, Kashyap K, Williams E, Aziz R, Schuler M, Ahamed C, et al. Analysis of 977 long COVID patients reveals prevalent neuropathy and association with antiganglioside antibodies. medRxiv [Preprint]. 2025 Mar 7. doi:10.1101/2025.03.04.25323101
- Ryan FJ, Hope CM, Masavuli MG, Ryan FJ, Hope CM, Masavuli MG, Lynn MA, Mekonnen ZA, Yeow AEL, et al. Long-term perturbation of the peripheral immune system months after SARS-CoV-2 infection. BMC Med. 2022;20(1):26. doi:10.1186/s12916-021-02228-6
- 870 55. Bosch JA, Berntson GG, Cacioppo JT, Dhabhar FS, Marucha PT. Acute stress evokes 871 selective mobilization of T cells that differ in chemokine receptor expression: a potential 872 pathway linking immunologic reactivity to cardiovascular disease. Brain Behav Immun. 873 2003;17(4):251-9. doi:10.1016/S0889-1591(03)00054-0
- Satarkar D, Patra C. Evolution, expression and functional analysis of CXCR3 in neuronal and cardiovascular diseases: a narrative review. Front Cell Dev Biol. 2022;10:882017. doi:10.3389/fcell.2022.882017
- 877 57. Blank T, Detje CN, Spieß A, Hagemeyer N, Brendecke SM, Wolfart J, et al. Brain endothelial- and epithelial-specific interferon receptor chain 1 drives virus-induced sickness behavior and cognitive impairment. Immunity. 2016;44(4):901-12. doi:10.1016/j.immuni.2016.04.005
- 881 58. Altara R, Manca M, Brandão RD, Zeidan A, Booz GW, Zouein FA. Emerging importance of chemokine receptor CXCR3 and its ligands in cardiovascular diseases. Clin Sci (Lond). 2016;130(7):463-78. doi:10.1042/CS20150666
- Yang J, Richmond A. The angiostatic activity of interferon-inducible protein-10/CXCL10 in human melanoma depends on binding to CXCR3 but not to glycosaminoglycan. Mol Ther. 2004;9(6):846-55. doi:10.1016/j.ymthe.2004.01.010
- Charfeddine S, Ibn Hadj Amor H, Jdidi J, Torjmen S, Kraiem S, Hammami R, et al. Long COVID-19 syndrome: is it related to microcirculation and endothelial dysfunction? Insights from TUN-EndCOV study. Front Cardiovasc Med. 2021;8:745758. doi:10.3389/fcvm.2021.745758
- Haunhorst S, Dudziak D, Scheibenbogen C, Seifert M, Sotzny F, Finke C, et al. Towards an understanding of physical activity-induced post-exertional malaise: insights into

- microvascular alterations and immunometabolic interactions in post-COVID condition and myalgic encephalomyelitis/chronic fatigue syndrome. Infection. 2024 Sep 6. doi:10.1007/s15010-024-02386-8
- Jacobs LMC, Wintjens MSJN, Nagy M, Willems L, Ten Cate H, Spronk HMH, et al.
 Biomarkers of sustained systemic inflammation and microvascular dysfunction
 associated with post-COVID-19 condition symptoms at 24 months after SARS-CoV-2
 infection. Front Immunol. 2023;14:1182182. doi:10.3389/fimmu.2023.1182182
- 900 63. Palma JA. Muscarinic control of cardiovascular function in humans: a review of current clinical evidence. Clin Auton Res. 2024;34(1):31-44. doi:10.1007/s10286-024-01016-902 5
- 903 64. Xie Y, Choi T, Al-Aly Z. Postacute sequelae of SARS-CoV-2 infection in the pre-Delta, 904 Delta, and Omicron eras. N Engl J Med. 2024;391(6):515-25. doi:10.1056/NEJMoa2403211
- 906 65. Fischer C, Willscher E, Paschold L, Gottschick C, Klee B, Diexer S, et al. SARS-CoV-907 2 vaccination may mitigate dysregulation of IL-1/IL-18 and gastrointestinal symptoms 908 of the post-COVID-19 condition. NPJ Vaccines. 2024;9(1):23. doi:10.1038/s41541-909 024-00815-1
- Achleitner M, Steenblock C, Dänhardt J, Jarzebska N, Kardashi R, Kanczkowski W, et
 al. Clinical improvement of long-COVID is associated with reduction in autoantibodies,
 lipids, and inflammation following therapeutic apheresis. Mol Psychiatry.
 2023;28(7):2872-7. doi:10.1038/s41380-023-02084-1
- Stein E, Heindrich C, Wittke K, Kedor C, Kim L, Freitag H, et al. Observational study
 of repeat immunoadsorption in post-COVID ME/CFS patients with elevated β2 adrenergic receptor autoantibodies—an interim report. J Clin Med. 2023;12(19):6428.
 doi:10.3390/jcm12196428
- 918 Hohberger B, Ganslmayer M, Harrer T, Kruse F, Maas S, Borst T, et al. Safety, 68. tolerability and clinical effects of rovunaptabin, also known as BC007 on fatigue and 919 quality of life in patients with Post-COVID syndrome (reCOVer): a prospective, 920 exploratory, placebo-controlled, double-blind, randomised phase IIa clinical trial 921 (RCT). EClinicalMedicine. 2025 Jul 22;86:103358. doi: 922 10.1016/j.eclinm.2025.103358. 923

924

925

Figure Legends

Figure 1: Suggestive autoantibodies (AABs) by sympathicus activation. During the discovery phase, levels of 14 previously described AABs were compared between patients with highest (top 20%, n=22) and lowest (lowest 20%, n=22) sympathicus activation determined based on normalized HF over 24h. Data is presented as mean ± SD. Between-group comparison was performed using unpaired two-sided t-test or Mann-Whitney-U Test in case of non-normal distribution. A p-value < 0.15 was accepted for the identification of suggestive AABs (green box) in the discovery phase.

Figure 2: Adaptive immune receptor repertoire sequencing of peripheral B and T cells. A) Normalized B-cell receptor (BCR) repertoire metrics of patients with PCS (n=34), severe (n=26) or moderate (n=28) acute COVID-19, after COVID-19 recovery (n=55) and pre-pandemic healthy individuals (HD; n=59). IGHV rearrangements with <98% identity to the germline configuration were considered somatically hypermutated. B) Principal component analysis (PCA) of BCR VJ gene. Statistics: Pillai-Bartlett test of multivariate analysis of variance (MANOVA) of all principal components. C) Mean frequency of IGHV gene usage as clustered (ward.D2, Canberra) heatmap. D) BCR repertoire metrics for the indicated PCS subsets. Dotted lines represent the mean of the HD cohort. E) Frequency of IGHV usage for the indicated PCS subsets. Dotted lines represent the respective mean frequency in HDs. F) Normalized T-cell receptor (TCR) repertoire metrics of patients with PCS (n=34), severe (n=26) or moderate (n=28) acute COVID-19, after COVID-19 recovery (n=55) and pre-pandemic healthy individuals (HD; n=59). G) PCA of TCR VJ gene usage. Statistics: Pillai-Bartlett test of multivariate analysis of variance (MANOVA) of all principal components. H) Mean frequency of TRBV gene usage as clustered (ward.D2, Canberra) heatmap. I) TCR repertoire metrics for the indicated PCS subsets. Dotted lines represent mean of the HD cohort. J) Frequency of TRBV usage for the indicated PCS subsets. Dotted lines represent the respective mean frequency in HDs. A/J) p-values indicate results of ANOVA. Otherwise not significant.

Figure 3: A) Levels auf autoantibodies (AABs) by type of care during acute COVID-19. Patients had either received ambulatory care at home (n=69), in-hospital care (hosp., n=9) or in-hospital care with ventilation (w. vent., n=21). A general trend to lower AAB levels with in-hospital acute care was observed, while the highest levels for CXCR3ab were detected in patients with ventilation. Data is presented as mean \pm SD. Multiple comparison was performed using ANOVA or non-parametric Kruskal-Wallis-Test and was significant for AGT1Rab (p=0.0227), ADRB1ab (p=0.0258), ADRB1ab (p=0.0109), and CXCR3ab (p=0.0007). The type of care during acute infection was not available/ unclear for six patients. B) Post-acute CXCR3ab levels. AAB levels against CXCR3 were significantly higher in patients with a more recent acute SARS-CoV-2 infection. No significant association of time after acute infection was detected for other AABs (all p > 0.05, data not shown). Trend line was modelled using third order polynomial nonlinear regression with 95% CI on individual data points (n=105).

Figure 4: Results of the logistic regression model based on autoantibodies (AABs). A) The model's performance was evaluated using the area under the receiver operating characteristic (ROC) curve (AUC) with HFnu 24h as a binary classifier. The AUC of 0.78 indicates moderate discriminative power. B) Confusion matrix indicating the model's prediction results in terms of true and false negatives/ positives. C) Feature importance chart indicating the contribution of each AAB to the model. A higher score indicates a larger effect on the model. All predictor variables (AABs) were standardized prior to modeling to ensure comparability. 10-fold cross-validation was used to assess the model's accuracy and mitigate the risk of overfitting.

Figure 5: Vasoactive capacity of autoantibodies (AABs). A) Higher mean arterial pressure (MAP) was detected in patients with high levels of CXCR3ab (n=27) during the day and night period as well as over 24h of blood pressure measurement compared to patients with low CXCR3 levels (n=79). Data is presented as mean ± SD. Between-group comparison was performed using ANOVA. **B)** AABs against ADRB1 did not affect exercise-induced HR response. The HR response during cardiopulmonary exercise testing (CPET) was effectively reduced by beta blocker medication. Neither patients with beta

blockers (BB+) nor patients without beta blockers (BB-) showed differences in HR response at ventilatory thresholds 1 or 2 (VT1, VT2) or peak exercise intensity (VO₂peak) depending on ADRB1ab levels. Peak heart rate was unaffected by the achieved load percentage (Watt) of the respective individual reference (corrected for age, sex and body surface area). CPET data is presented as mean and 95% CI over three time points compared by two-way ANOVA (for time x beta blocker group) and mean ± SD for HR peak data compared by ANOVA. C-E) Higher AAB levels enhance the blood pressure response during physical exercise. Patients with higher levels of AGT1Rab (n=20) had an increased diastolic blood pressure (DBP) response during cardiopulmonary exercise testing (CPET) compared to patients with lower levels (n=85). Patients with elevated M1Rab and CXCR3ab levels (n=25, n=27) showed higher DBP and also mean arterial pressure (MAP) values during CPET compared to patients with lower levels (n=85, n=78). Patients with higher CXCR3ab levels also showed reduced blood oxygen saturation (SPO₂) during exercise testing. For comparison, patients individual relative load was calculated and third order polynomial curve fit with 95% CI with F statistics for comparison of curve fit was used based on multiple BP and SPO₂ measurements during the test. P-values < 0.05 indicate that curves are significantly different and do not fit the compared datasets. The mean of all measurements combined was compared between groups using unpaired two-sided t-test or Mann-Whitney-U Test in case of non-normal distribution. Red color indicates high AAB levels, green color indicates low AAB levels.

Figure 6: Time-dependent in vitro cell response profiling to patients' serum by real-time cell electronic sensing. A) Schematic presentation of real-time cell electronic sensing analysis of serum effects on human induced pluripotent stem cell (hiPSC) derived cardiomyocyte (CM) contraction profiles. Three different serotypes were used, high autoantibody (high AA), low autoantibody (low AA) and CXCR3 negative high autoantibody (CXCR3 neg high AA). B) Cell Index curves indicating the initial adhesion of the hiPSC-cardiomyocytes and decline in Cell Index after serum stimulation (1% serum at day 6). The curve represents the mean Cell Index value \pm SD (n = 26-52 wells from three individual experiments). a.u = arbitrary units; ****p < 0.001; Tukey's multiple-comparisons test was performed to calculate significance between the groups compared to untreated (1% medium control). C) comparison of cell contractility (beats per minute, bpm) and D) amplitude of hiPSC-cardiomyocytes with or without serum stimulation on day 7 (n = 24-43 wells from three individual experiments). a.u = arbitrary units; all data are represented as mean \pm SD; **p < 0.01; ****p < 0.001; ns = not significant; Dunnett's T3 (Brown-Forsythe and Welch ANOVA) multiple-comparisons test was performed.

TABLES

Table 1: Exercise capacity assessed by cardiopulmonary exercise testing (CPET)

	absolute	% predicted
Resting		
Heart rate, beat-min ⁻¹	89.3 ± 11.2	n.a.
O ₂ pulse, ml·beat ⁻¹	6.7 ± 1.9	n.a.
Systolic blood pressure, mmHg	125.7 ± 20.8	n.a.
Diastolic blood pressure, mmHg	79.3 ± 14.1	n.a.
SpO ₂ , %	94.8 ± 10.3	n.a.
Ventilatory threshold 1 (VT1)		
Workload, watt	69.6 ± 25.5	39.8 ± 14.5
Heart rate, beat⋅min ⁻¹	109.0 ± 15.0	65.2 ± 8.2
O ₂ pulse, ml·beat ⁻¹	10.3 ± 2.9	75.0 ± 15.2
Systolic blood pressure, mmHg	146.6 ± 25.3	71.0 ± 12.3
Diastolic blood pressure, mmHg	79.6 ± 15.6	80.6 ± 15.7
VO ₂ , ml·min ⁻¹ ·kg ⁻¹	12.1 ± 3.0	49.5 ± 13.5
SpO ₂ , %	92.8 ± 17.3	97.5 ± 18.3
Peak exercise (VO _{2peak})		
Workload, watt	120.5 ± 32.9	69.6 ± 19.7
Heart rate, beat-min ⁻¹	134.1 ± 21.6	80.0 ± 11.8
O ₂ pulse, ml·beat ⁻¹	12.3 ± 3.0	90.1 ± 15.7
Systolic blood pressure, mmHg	174.8 ± 30.3	84.5 ± 14.6
Diastolic blood pressure, mmHg	86.2 ± 16.0	87.3 ± 15.8
VO ₂ , ml·min ⁻¹ ·kg ⁻¹	17.8 ± 4.0	72.0 ± 15.3
SpO ₂ , %	95.4 ± 3.9	100.4 ± 4.0
Rating of perceived exertion (0 – 10 Borg Scale)	9 (5)	n.a.

Data is presented as mean ± SD or median (range) at admission (available for n=93 patients). % predicted values indicate reference values corrected for sex, age and body surface area. N.a., not applicable.

Table 2: Correlation of heart rate variability (HRV) variables with autoantibodies by 24h, day, and night period

			Autoantibody							
		AGT1Rab	AGT2Rab	ADRB1ab	ADRB2ab	M1Rab	M3Rab	CXCR3ab	PAR1ab	
		1			Time-related va	riables (24h)		1	l	
SDNN, ms	Spearman's Rho	0.186	-0.070	0.090	0.119	-0.067	0.134	-0.045	0.002	
	p-value	0.058	0.476	0.360	0.227	0.500	0.175	0.651	0.980	
SDANN, ms	Spearman's Rho	0.115	-0.081	0.020	0.059	-0.074	0.063	-0.049	-0.031	
	p-value	0.242	0.411	0.836	0.550	0.453	0.523	0.623	0.754	
SDNN Index, ms	Spearman's Rho	0.255**	-0.126	0.161	0.164	-0.171	0.217*	-0.138	-0.081	
	p-value	0.009	0.199	0.100	0.094	0.082	0.026	0.161	0.411	
rMSSD, ms	Spearman's Rho	0.269**	-0.078	0.223*	0.239*	-0.055	0.248*	-0.106	0.079	
	p-value	0.006	0.426	0.022	0.014	0.576	0.011	0.282	0.420	
pNN50, %	Spearman's Rho	0.301**	-0.098	0.247 [*]	0.244*	-0.104	0.246 [*]	-0.110	-0.014	
	p-value	0.002	0.319	0.011	0.012	0.290	0.011	0.265	0.887	
Triangular Index	Spearman's Rho	0.114	0.020	0.043	0.082	-0.073	0.122	-0.105	-0.072	
	p-value	0.247	0.840	0.665	0.406	0.459	0.215	0.286	0.464	
		1		Fre	quency-related	l variables (2	4h)			
LF Power, ms ²	Spearman's Rho	0.234*	-0.196*	0.116	0.131	-0.305**	0.204*	-0.142	-0.164	
	p-value	0.016	0.045	0.239	0.183	0.002	0.037	0.148	0.094	
HF Power, ms ²	Spearman's Rho	0.259**	-0.092	0.205*	0.216 [*]	-0.131	0.214*	-0.246*	-0.075	

	p-value	0.008	0.350	0.036	0.027	0.183	0.028	0.011	0.447
LF/HF Ratio	Spearman's Rho	-0.169	-0.115	-0.232*	-0.229*	-0.105	-0.156	0.221*	-0.096
	p-value	0.084	0.241	0.017	0.019	0.288	0.112	0.023	0.330
LFnu	Spearman's Rho	-0.217 [*]	-0.139	-0.273**	-0.280**	-0.088	-0.214*	0.181	-0.121
	p-value	0.026	0.157	0.005	0.004	0.372	0.029	0.064	0.218
HFnu	Spearman's Rho	0.163	0.111	0.227*	0.224*	0.100	0.150	-0.230*	0.083
	p-value	0.097	0.259	0.020	0.022	0.310	0.127	0.018	0.400
Sympathetic %nu	Spearman's Rho	-0.170	-0.117	-0.232*	-0.229*	-0.106	-0.157	0.220*	-0.096
	p-value	0.083	0.233	0.017	0.019	0.280	0.110	0.024	0.329
Parasympathetic %nu	Spearman's Rho	0.170	0.117	0.232*	0.229*	0.106	0.157	-0.220*	0.096
	p-value	0.083	0.233	0.017	0.019	0.280	0.110	0.024	0.329
					Non-linear va	riables (24h)			
SD1, ms	Spearman's Rho	0.284**	-0.068	0.230*	0.254**	-0.072	0.223*	-0.182	0.021
	p-value	0.003	0.493	0.019	0.009	0.470	0.023	0.065	0.832
SD2, ms	Spearman's Rho	0.184	-0.062	0.084	0.121	-0.075	0.125	-0.049	-0.006
	p-value	0.062	0.534	0.398	0.223	0.452	0.206	0.620	0.950
VAI, °	Spearman's Rho	0.461**	0.005	0.423**	0.426**	0.003	0.380**	-0.021	0.095
	p-value	0.0001	0.959	0.0001	0.0001	0.974	0.0001	0.831	0.339
	•			Т	ime-related vai	riables (6h da	y)		
SDNN, ms	Spearman's Rho	0.226*	-0.007	0.084	0.124	-0.081	0.187	-0.039	0.024
	p-value	0.020	0.942	0.395	0.209	0.409	0.057	0.694	0.810

rMSSD, ms	Spearman's Rho	0.250 [*]	-0.086	0.203*	0.220 [*]	-0.078	0.225*	-0.115	0.044
	p-value	0.010	0.386	0.038	0.024	0.432	0.021	0.242	0.654
pNN50, %	Spearman's Rho	0.318**	-0.086	0.248 [*]	0.248*	-0.127	0.264**	-0.103	-0.001
	p-value	0.001	0.386	0.011	0.011	0.198	0.007	0.296	0.992
				Frequer	cy-related vari	ables (6h day)		
LF Power, ms ²	Spearman's Rho	0.210 [*]	223 [*]	0.113	0.116	-0.313**	0.193 [*]	-0.179	-0.207 [*]
	p-value	0.032	0.023	0.253	0.237	0.001	0.049	0.068	0.034
HF Power, ms ²	Spearman's Rho	0.236*	-0.112	0.208 [*]	0.210*	-0.161	0.202*	-0.298**	-0.120
	p-value	0.015	0.253	0.033	0.031	0.100	0.039	0.002	0.224
LF/HF Ratio	Spearman's Rho	-0.172	-0.135	-0.238*	-0.232*	-0.125	-0.161	0.172	-0.145
	p-value	0.079	0.169	0.015	0.017	0.205	0.100	0.079	0.140
LFnu	Spearman's Rho	-0.183	-0.184	-0.256**	-0.253**	-0.167	-0.181	0.143	-0.169
	p-value	0.062	0.060	0.008	0.009	0.089	0.064	0.144	0.086
HFnu	Spearman's Rho	0.125	0.052	0.172	0.166	0.051	0.099	-0.200*	0.103
	p-value	0.202	0.597	0.079	0.090	0.606	0.315	0.041	0.294
Sympathetic %nu	Spearman's Rho	-0.172	-0.135	-0.238 [*]	-0.232*	-0.125	-0.161	0.172	-0.145
	p-value	0.079	0.169	0.015	0.017	0.205	0.100	0.079	0.140
Parasympathetic %nu	Spearman's Rho	0.172	0.135	0.238*	0.232*	0.125	0.161	-0.172	0.145
	p-value	0.079	0.169	0.015	0.017	0.205	0.100	0.079	0.140
				Ti	me-related vari	iables (6h nigl	ht)		
SDNN, ms	Spearman's Rho	0.203*	-0.009	0.088	0.123	-0.020	0.162	-0.013	0.041

	p-value	0.038	0.924	0.369	0.210	0.838	0.099	0.897	0.680
rMSSD, ms	Spearman's Rho	0.254**	-0.064	0.201*	0.215*	0.023	0.199*	-0.073	0.066
	p-value	0.009	0.515	0.040	0.027	0.820	0.041	0.457	0.505
pNN50, %	Spearman's Rho	0.253**	-0.029	0.221*	0.226*	-0.051	0.236*	-0.114	0.000
	p-value	0.009	0.767	0.024	0.020	0.609	0.015	0.248	0.996
				Frequen	cy-related varia	ıbles (6h nigh	it)		
LF Power, ms ²	Spearman's Rho	0.264**	-0.096	0.136	0.164	-0.176	0.206*	-0.031	-0.043
	p-value	0.006	0.329	0.166	0.094	0.073	0.035	0.753	0.662
HF Power, ms ²	Spearman's Rho	0.222*	-0.046	0.168	0.183	-0.079	0.187	-0.161	-0.042
	p-value	0.023	0.642	0.086	0.062	0.424	0.056	0.100	0.668
LF/HF Ratio	Spearman's Rho	-0.143	-0.093	-0.204*	-0.195 [*]	-0.074	-0.156	0.204*	-0.032
	p-value	0.145	0.345	0.037	0.046	0.455	0.111	0.037	0.742
LFnu	Spearman's Rho	-0.160	-0.121	-0.224 [*]	-0.209*	-0.098	-0.180	0.182	-0.063
	p-value	0.104	0.220	0.022	0.034	0.324	0.067	0.065	0.525
HFnu	Spearman's Rho	0.157	0.108	0.221*	0.211*	0.096	0.161	-0.192	0.044
	p-value	0.112	0.274	0.024	0.031	0.333	0.103	0.051	0.657
Sympathetic %nu	Spearman's Rho	-0.143	-0.093	-0.204*	-0.195 [*]	-0.074	-0.156	0.204*	-0.032
	p-value	0.145	0.345	0.037	0.046	0.455	0.111	0.037	0.742
Parasympathetic %nu	Spearman's Rho	0.143	0.093	0.204*	0.195*	0.074	0.156	-0.204*	0.032
	p-value	0.145	0.345	0.037	0.046	0.455	0.111	0.037	0.742

Blue: positive correlation, red: negative correlation, darker colors indicate stronger correlation.

